

# Coherent transport in graphene nanoconstrictions

F. Muñoz-Rojas, D. Jacob, J. Fernández-Rossier\* , and J. J. Palacios

*Departamento de Física Aplicada, Universidad de Alicante, San Vicente del Raspeig, SPAIN*

(Dated: July 5, 2018)

We study the effect of a structural nanoconstriction on the coherent transport properties of otherwise ideal zig-zag-edged infinitely long graphene ribbons. The electronic structure is calculated with the standard one-orbital tight-binding model and the linear conductance is obtained using the Landauer formula. We find that, since the zero-bias current is carried in the bulk of the ribbon, this is very robust with respect to a variety of constriction geometries and edge defects. In contrast, the curve of zero-bias conductance versus gate voltage departs from the  $(2n + 1)e^2/h$  staircase of the ideal case as soon as a single atom is removed from the sample. We also find that wedge-shaped constrictions can present non-conducting states fully localized in the constriction close to the Fermi energy. The interest of these localized states in regards the formation of quantum dots in graphene is discussed.

PACS numbers:

## I. INTRODUCTION

The recent fabrication of field effect transistor devices based both upon quasi-2D graphite quantum dots<sup>1</sup> and upon graphene<sup>2,3,4</sup> (a single atomic layer of graphite), and the observation of a new type of quantum Hall effect in the latter have triggered a huge interest in the electronic properties of this system. Most of the results of standard mesoscopic physics need to be revisited<sup>5,6,7</sup> in the case of graphene because its electronic structure is fundamentally different from that of metals and semiconductors where either a large density of states (DOS) at the Fermi energy or a large gap determine the properties of the materials. Graphene is a semimetal with zero DOS at the Fermi energy and zero gap. On top of that, the electronic structure close to the Fermi energy has a conical shape with perfect electron-hole symmetry, identical to that of two dimensional massless Dirac fermions<sup>8</sup>.

Here we consider graphene-based one dimensional flat structures, the so called graphene nano-ribbons<sup>9,10,11,12</sup>. As opposed to two dimensional graphene, ribbons can present a finite density of states at the Fermi energy which dominates electrical transport in undoped or weakly doped samples. Ideal graphene ribbons can be considered as the flat parent structures of carbon nanotubes, whose electronic properties have been thoroughly studied<sup>14</sup>. Electronic transport in carbon nanotubes has been studied in different regimes, including ballistic<sup>15</sup>, Coulomb Blockade<sup>16</sup> and Kondo<sup>17,18</sup>. Progress in the fabrication of graphene based nano-structures that permits to study transport in graphene ribbons motivates this work.

The presence of edges makes the electronic structure of graphene ribbons different from that of nanotubes. Two types of idealized edges are usually considered: Armchair and zig-zag<sup>9</sup>. Interestingly, all the zig-zag and

some of the armchair edges result in a band at the Fermi energy<sup>9</sup>. In the case of narrow zig-zag-edged ribbons, the top and bottom edge states can be sufficiently close as to make hybridization possible, resulting in two low energy dispersive bands, symmetrically placed around the Fermi energy,  $E = 0$ . Depending on their width, nano-ribbons with armchair edges can be metallic or insulating. The different density of states for armchair and zig-zag edges has been experimentally observed in Scanning Tunnel Microscope (STM) experiments with atomic resolution<sup>19,20</sup>.

Coherent or quantum transport in graphene ribbons has been studied previously, both for ideal<sup>13</sup> and defective<sup>21,22</sup> cases in the infinite length  $L$  case. The case of disorder free graphene ribbons with finite  $L$  comparable to the width  $W$  has also been studied in connection with the experimental measurement of a minimum conductivity in mesoscopic size graphene layers<sup>5,6</sup>. In the spirit of quantum point contact physics, in this work we study the coherent transport of infinitely long graphene ribbons, narrower than  $W \simeq 5\text{nm}$ , with a structural nanometric constriction like the one schematically shown in Fig. (1). This type of structure can also be considered as an idealization of an all-carbon single-molecule junction. In conventional single-molecule junctions the organic molecule is attached to metallic electrodes. Here these are replaced by perfect graphene ribbons and the role of the molecule is played by a geometrical constriction. Due to the very different electronic structure displayed by different all-carbon nano-structures<sup>14</sup> the conduction properties of these systems do not appear obvious *a priori* to us.

We calculate the electronic structure in the one orbital tight binding approximation. The relevant orbital is the  $p_z$ , since the  $sp^2$  orbitals form bonding and anti-bonding states very far away in energy. In the TB approximation ideal two dimensional graphene has a conical energy dispersion at low energies and the Fermi surface ( $E = 0$ ) is formed by six points. This low energy region can be described in terms of a  $\vec{k} \cdot \vec{p}$  theory whose mathematical

---

\*jfrossier@ua.es

structure is very similar to the Dirac theory for massless fermions<sup>8</sup>, which yields physical insight. The  $\vec{k} \cdot \vec{p}$  has also been worked out for edge states in ideal ribbons<sup>12</sup>. The TB approach provides natural energy and momentum cutoffs to the  $\vec{k} \cdot \vec{p}$  theory, permits to model perturbations at the atomic scale and is a good preliminary step towards ab-initio calculations<sup>23</sup>.

The rest of the paper is organized as follows. In section II we review the transport formalism. In section III we review the electronic structure of ideal ribbons and we study the effect of vacancies, located at the edge of the ribbons, on their transport properties. We find that the conductivity of undoped graphene ribbons is weakly affected by the presence of this kind of disorder. In section IV and V we study transport properties of square- and wedge-shaped constrictions. Whereas the former present finite conductance, the latter have a vanishing transmission at low energies, coexisting with a finite density of localized states. These states at energies close to zero form what can be called a quantum dot in graphene. In section VI we discuss the validity of our approximations and we summarize and discuss the main results of this manuscript.

## II. TRANSPORT THEORY

The natural framework for transport calculations in nanoscopic devices is the Landauer formalism. The description of electron transport within the Landauer formalism is based on the assumption that transport across the highest resistance region is coherent, i.e., inelastic scattering is negligible there. A more complete account can be found, e.g., in the book by Datta<sup>24</sup>. In what follows we will assume that the inelastic mean free path for graphene electrons is much longer than the typical dimensions of the nanoconstrictions considered and than the ribbon widths. According to recent theory work, inelastic scattering due to phonons is very inefficient in graphene ribbons so that our assumption seems to be met even at room temperature<sup>25</sup>. This makes elastic scattering the major contributor to resistance. In contrast to metallic systems where the resistance of the electrodes is negligible compared to that of the nanoconstriction, in the case of graphene nanoconstrictions, the low-bias conductance of the ideal electrode is also very small,  $\frac{2e^2}{h}$ . The consequences of this are explored in what follows.

We consider the effect of constrictions on the transport properties of an otherwise ideal ribbon (Fig. 1). The system has three regions: the central region (or device) where the constriction is located and the left and right leads. The latter are described as semi-infinite one-dimensional perfect ribbons of finite width, characterized by the number of atoms in the unit cell,  $N$ . We only consider ribbons with zig-zag edges as the ones studied in previous works<sup>9,10,21</sup>. We consider constrictions of various shapes, from the removal of a single atom or a few atoms on the edge to square-shaped and wedge-shaped

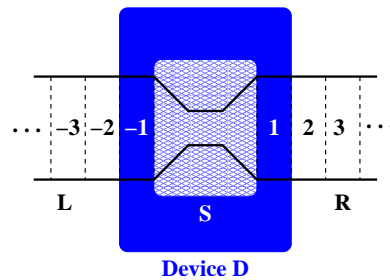


FIG. 1: Division of system into leads L and R, device D, and scattering region S (LEFT). And division of operator matrices into corresponding submatrices (RIGHT).

constrictions.

The introduction of the constriction breaks the translational symmetry of the perfect lead so that, in general, electrons incident on a given band will be either reflected or transmitted into other bands after hitting the constriction. The square of the transmission amplitude  $t_{nm}$  gives the probability of an incoming mode  $m$  to be scattered on an outgoing mode  $n$ . The Landauer formula links the overall transmission

$$T(E) = \sum_{m,n} \|t_{nm}\|^2 = \text{Tr}[t^\dagger t]$$

with the linear conductance

$$G(E_F) = \frac{2e^2}{h} T(E_F)$$

where  $E_F$  is the Fermi energy.

For completeness, we review the basic steps in the calculation of the transmission  $T(E)$  using single-particle Green's functions as routinely done in nanoelectronics<sup>24</sup>. In the TB approach used here, the Hamiltonian matrix is straightforwardly obtained for a given atomic structure. The leads are characterized by a unit cell with  $N$  atoms and a propagation direction which we take along the  $x$  axis. When written in blocks  $N \times N$ , the Hamiltonian of the leads is a semi-infinite tridiagonal matrix, with intra-cell blocks  $H_0$  and an inter-cell first-neighbor coupling  $V$ . Our starting point is the partition of the Hamiltonian of the infinite system in 3 regions. The choice of the boundaries between device and leads is done so that left and right electrodes are not directly coupled. For convenience the device region is always chosen so that the left and right boundaries are given by one of these units cells. Therefore, the coupling between the surface unit cell of the left (right) electrode to the right (left) boundary of the device is given by the same inter-cell matrix  $V$ . According to this scheme, the Hamiltonian matrix set is divided into submatrices as follows:

$$H = \begin{pmatrix} H_L & H_{LD} & 0 \\ H_{DL} & H_D & H_{DR} \\ 0 & H_{RD} & H_R \end{pmatrix}, \quad (1)$$

Here  $H_D$  is a finite size square matrix with range equal to the number of atoms in the device,  $N_d$ . In contrast,

$H_{L,R}$  are infinite size square matrices describing the semi-infinite electrodes and  $H_{DL}$  and  $H_{LD}$  are infinite rectangular matrices. The Green function operator, defined as

$$(E - H)G(E) = 1 \quad (2)$$

can also be divided into submatrices as:

$$G = \begin{pmatrix} G_L & G_{LD} & G_{LR} \\ G_{DL} & G_D & G_{DR} \\ G_{RL} & G_{RD} & G_R \end{pmatrix}. \quad (3)$$

After simple steps, it is possible to write the Green function of the device as:

$$G_D(E) = (E - H_D - \Sigma_L(E) - \Sigma_R(E))^{-1}. \quad (4)$$

where  $\Sigma_{L,R}$  are the so called self-energy  $N_d \times N_d$  matrices given by

$$\begin{aligned} \Sigma_L(E) &:= H_{DL} g_L(E) H_{LD} \\ \Sigma_R(E) &:= H_{DR} g_R(E) H_{RD} \end{aligned} \quad (5)$$

The selfenergies  $\Sigma_L(E)$  and  $\Sigma_R(E)$  describe the effect of the electrodes on the electronic structure of the *device*. The real part of the self-energy results in a shift of the device levels whereas the imaginary part provides a lifetime. The device self-energies are given by the Green's functions of the semi-infinite isolated leads  $g_L(E) = (E - H_L)^{-1}$  and  $g_R(E) = (E - H_R)^{-1}$  projected into the device region by the coupling of the leads to the device  $H_{DL}$  and  $H_{RD}$ . In contrast to the Green function of an infinite system with translational invariance, the calculation of the Green function of a semi-infinite system with a surface is non-trivial.

We can write the surface part of the semi-infinite Green function  $g_{L,R}(E)$  of the electrode as:

$$g_{L,R}(E)|_{\text{surface}} = \frac{1}{E - H_0 - \Sigma_{l,r}(E)}, \quad (6)$$

where  $\Sigma_{l,r}$  is a self-energy (different from  $\Sigma_{L,R}$ ) that accounts for the effect of the rest of the semi-infinite chain on the first unit cell. In one dimension it is possible to derive a recursive relation that yields a self-consistent Dyson equation for this self-energy:

$$\Sigma_{l,r}(E) = V \frac{1}{E - H_0 - \Sigma_{l,r}(E)} V^\dagger. \quad (7)$$

The coupling matrices  $\Gamma_L(E)$  and  $\Gamma_R(E)$  are defined as the difference between the retarded and advanced self-energy of the leads projected into the device by the coupling  $H_{DL}$  and  $H_{RD}$ :

$$\Gamma(E)_{L(R)} = i \left( \Sigma_{L(R)}(E) - \Sigma_{L(R)}^\dagger(E) \right). \quad (8)$$

With all these ingredients, we can compute the transmission using the result<sup>24</sup>:

$$T(E) = \text{Tr}[\Gamma_L(E) G_D^\dagger(E) \Gamma_R(E) G_D(E)]. \quad (9)$$

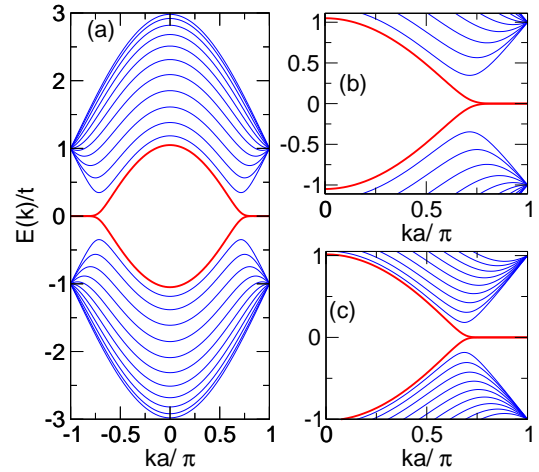


FIG. 2: (a) Bands of the ideal zig-zag ribbon with 24 atom unit cell. (b) Detail of the low energy sector. (c) Detail of the low energy sector for the 48 atom unit cell

Therefore, for a given system, we first compute the electrode surface Green function (6) by solving the Dyson equation (7). This permits to compute the device self-energy (5), the device Green function (4) and the coupling matrices (8). The final step is the calculation of the transmission function.

### III. IDEAL AND WEAKLY DEFECTIVE ZIG-ZAG RIBBONS

#### A. Ideal ribbons

In this section we briefly review the electronic structure and transport properties of both ideal and weakly defective zig-zag-edged ribbons. We consider ribbons with two different widths whose unit cells are composed of  $N = 24$  and  $N = 48$  atoms, respectively. The super-cell unit of the  $N = 24$  ribbon is shown in Fig. (3b). The honeycomb lattice of 2D infinite graphene can be generated by a triangular lattice of unit cells with two atoms, labeled  $A$  and  $B$ . Therefore, the honeycomb lattice is formed by two interpenetrating sub-lattices,  $A$  and  $B$ . The first neighbors of atoms in the lattice  $A$  belong to sub-lattice  $B$  and vice versa. This underlying structure is responsible for most of the peculiar features of graphene electronic structure. Nano-ribbons inherit these properties and, in the case of zig-zag nano-ribbons, the top and bottom edges belong to atoms on different sublattices<sup>12</sup>.

Figure (2) shows the band structure for the  $N = 24$  case [Figs. 2(a) and 2(b)] and for the  $N = 48$  case [only the low energy region is now shown in Fig. 2(c)]. The energy units are given in terms of the hopping parameter  $|t| \simeq 3\text{eV}$  which is the only energy scale in the Hamiltonian. There is a perfect electron-hole symmetry which sets the Fermi energy to zero for half filling. Notice that the density of bands per energy interval is largest for the

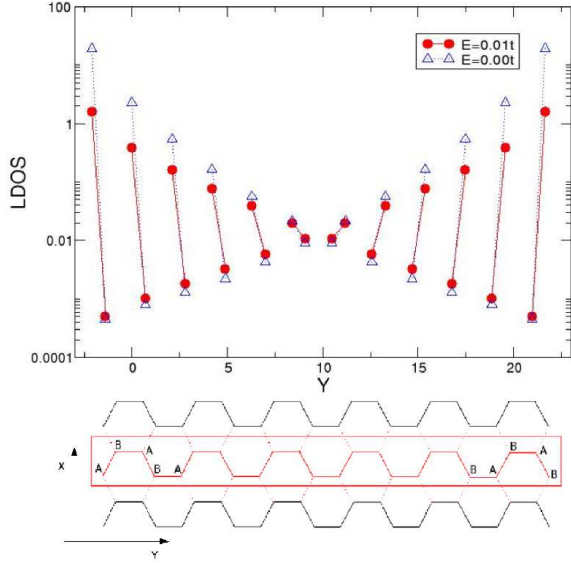


FIG. 3: Upper panel: Local density of states of the ideal 24 atoms-wide ribbons for  $E = 0$  (circles) and  $E = 0.01t$  (triangles). Notice the vertical logarithmic scale. Lower panel: atomic structure of a section of a  $N = 24$  zig-zag ribbon.

wider ribbon, as expected. We can distinguish three different regions, (i)  $|E| < \Delta_1$ , (ii)  $\Delta_1 < |E| < |t|$  and (iii)  $|E| > t$ , where  $\Delta_1$  is the minimum energy of the second sub-band closest to  $|E| = 0$ . This energy scale  $\Delta_1$  is associated to the finite width of the ribbon and it decreases as  $N^{-1}$ . For the cases considered here,  $N = 24$  and  $N = 48$ ,  $\Delta_1 = 0.35t$  and  $\Delta_1 = 0.18t$  respectively. In the  $N = \infty$  limit  $\Delta_1$  goes to zero, as expected for two-dimensional graphene.

The density of extra carriers that needs to be injected in the ribbon so that the Fermi energy hits the second subband,  $E_F = \Delta_1$ , exceeds the upper experimental limit reached so far<sup>1</sup>,  $\delta n = 10^{13} \text{ cm}^{-2}$ . Electrical doping up to the second subband could be possible for wider ribbons. Although only the lowest energy region  $|E| < \Delta_1$  could be accessible experimentally for the narrow ribbons considered here, some insight can be gained also by analyzing the effect of elastic scattering on the transmission at energies in the other two regions. The bands immediately above  $\Delta_1$  present two positive (and two negative) momenta at a given energy. This results in the doubling of the number of conducting channels at a given energy, as long as  $|E| < t$ . Higher in energy,  $|E| > t$ , we find simple parabolic bands which yield one channel per band as in the case of III-V semiconductors.

The energy bands closest to  $E_F$  are flat for  $|k|$  larger than a critical wave-vector  $k_c$ , and present dispersion otherwise. The cutoff  $k_c$  is a decreasing function of  $N$  which tends to  $k_c a / \pi = 2/3$  in the  $N = \infty$  limit<sup>9</sup>. In figure 3 we plot the local density of states across a super-cell unit for the ribbon with  $N = 24$  and for two different energies,  $E = 0$  and  $E = 0.01t$ . Atoms  $A$  and  $B$  in the same unit cell are joined by a straight line. In both cases the LDOS

is peaked on the edges, although the contrast is larger for the  $E = 0$  case, which corresponds to the dispersionless states. The LDOS presents a peculiar oscillation, related to the sub-lattice structure. Starting from the left edge, the LDOS peaks only in  $A$ , the weight on the first  $B$  atom being very small. As we move towards the center the weight on  $A$  atoms decays exponentially whereas the weight on the  $B$  atoms increases exponentially. In the center the weight on the  $A$  and  $B$  atoms is comparable and the weight on the  $B$  atoms becomes dominant as we move towards the opposite edge, in very good agreement with the  $\vec{k} \cdot \vec{p}$  theory<sup>12</sup>. As a result, the density of states, disregarding the sub-lattice index, is peaked at the edges, which permits to refer to the lowest subband states as "edge states".

It is apparent from Fig. 3 that the  $A$  and  $B$  edge states become coupled in the middle of the ribbon. Importantly, the structure of the current operator is the same as the hopping part of the Hamiltonian, coupling atoms of the different sub-lattices. Therefore, the current density of a given state, evaluated in a unit cell with two atoms, is proportional to the product of its  $A$  and  $B$  components,  $\psi_A(y)$  and  $\psi_B(y)$ . In the continuum limit the current associated to the wave function  $\Psi^\dagger = (\psi_A^*, \psi_B^*)$  reads  $j_x(y) \propto (\Psi^\dagger \sigma_x \Psi)$ , where  $\sigma_x$  is the Pauli matrix acting on the  $AB$  space<sup>5,6,26</sup>. From figure (3) we expect that the product  $\psi_A(y) \times \psi_B(y)$  to take similar values in the edges<sup>12</sup> and in the center of the ribbon. The resulting picture is the following: whereas the charge density of low energy states, proportional to  $\rho(y) = |\psi_A|^2 + |\psi_B|^2$ , is peaked on the edges, their current density  $j_x(y)$  is more homogeneously distributed across the ribbon. This picture is substantially different from that of non-relativistic electrons with scalar wave functions  $\phi(x, y) = \psi(y)e^{ikx}$  for which the charge density  $\rho(y) = |\psi(y)|^2$  and the current density  $j_x(y) \propto \phi \partial_x \phi^* - \phi^* \partial_x \phi \propto k\rho(y)$  have the same profile. The consequences of this difference between the current and charge densities will become apparent later and are one of the results of this work.

## B. Defective edges

We now study the effect of a single vacancy in the edge(s) of the ribbon on the transport properties. From the formal point of view this is done using the approach described in the previous section. The sector of the ribbon where the vacancy is located is treated as the device. In Fig. 4 we plot  $T(E)$  for three cases: Ideal case, one atom missing and two atoms missing. As everywhere else in the text, this is the transmission per spin channel. Since we assume that time-reversal symmetry is not broken, the total transmission should be multiplied by a factor of 2 to account for the spin degree of freedom. All of them display electron-hole symmetry around  $E = 0$ . As in the case of the energy bands, the  $T(E)$  curves have three different regions. In the large  $|E|$  region, the transmission for the ideal ribbon  $T_{\text{ideal}}(E)$  is quantized ac-

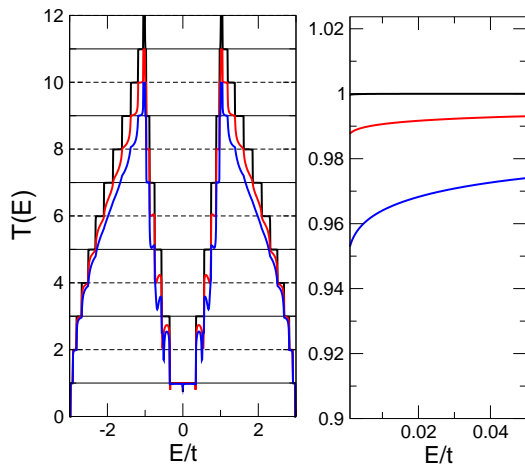


FIG. 4: (Color on-line). (a) Transmission spectrum for ribbons with  $N = 24$  atoms in the ideal case (black), removing 1 atom from the edge (red), and removing 2 atoms on the top and bottom edges (blue). (b) Detail of the transmission in the low energy sector. The effect of removing 1 or 2 atoms on the border is very small in the lowest conductance plateau.

cording to the usual law for non-relativistic electrons and holes:  $ne^2/h$ , where  $n$  is the number of bands that intersect the Fermi energy for  $k > 0$ . In this case  $n$  goes from 1 to 12 in steps of 1, consistent with the parabolic dispersion away from the Dirac cones. This large  $|E|$  region is not likely to be reached experimentally since it would imply a huge depletion of the charge, but is interesting from the conceptual point of view. In the intermediate region ( $t < |E| < \Delta_1$ )  $T_{\text{ideal}}(E)$  changes according to the rule  $(2n+1)e^2/h$ . This result has been previously obtained by Peres et al. (13). The factor of two comes from the shape of the bands in this region, as discussed above. The transmission is maximal at the energy where the "Dirac" ladder and the non-relativistic ladder meet at  $E \simeq t$ . In the relevant low energy sector, where we will focus our attention from now on, the transmission of the ideal ribbon is one.

The effect of scattering introduced in the ribbons affects very differently the transmission in the different energy regions. The removal of a *single* atom on the edge erases the  $2n+1$  ladder in the intermediate energy region for the  $N = 24$  ribbon [see Fig. 4(a)]. This points towards a very difficult experimental verification of the  $2n+1$  transmission ladder in these narrow ribbons. In contrast, in the case of  $N = 48$  the conductance remains quantized in the  $2n+1 = 3$  plateau after the removal of 1 atom in each edge, but the higher energy plateaus disappear.

In contrast with the higher energy subbands ( $|E| > \Delta_1$ ), the plateau in the low energy sector is only weakly affected by the removal of atoms in the edges, even for the narrower ribbon ( $N = 24$ ) as can be seen in Fig. 4(b). The effect on the transmission in the experimentally relevant low energy sector is below two percent for the removal of one atom on one edge and below five per-

cent when one atom is missing on both edges. In contrast, the removal of a single atom in the central part of the ribbon (not shown) has a much larger influence on the low energy transmission. These results are compatible with the fact that the current density carried by edge states is spread along the central region. The robustness of the transmission in the low energy sector and its weakness in the intermediate energy sector are relevant results since atomic size fluctuations in the edges are unavoidable in real samples.

#### IV. SQUARE CONSTRICTIONS

We now present results for square-shaped nanoconstrictions as those shown in Fig. 5. We choose this shape because it permits a comparison with a simple model for electrons in parabolic bands. It also seems possible to obtain analytical expressions for the transmission curve for square constrictions using analytical approach along the lines of previous work<sup>5,6,12</sup>. Another feature of square constrictions is the presence of armchair edges joining the zig-zag edges of the wide and narrow regions. We consider square constrictions with top-bottom symmetry, like those in the Fig. (5), characterized by three lengths: The width of the electrode and the width of the constriction,  $N$  and  $N_c$ , both measured in units of the number of atoms of the super-cell unit, and the length of the constriction  $L$ , measured in units of  $a$ , the graphene lattice parameter.

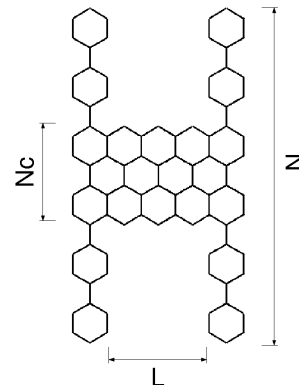


FIG. 5: (Color On-line). Structure of the square-shape nanoconstriction with 3 characteristic lengths,  $N$ ,  $N_c$  and  $L$ .

In Fig. (6) we show transmission curves for a variety of square constrictions. In Figs. 6(a) and (b) we show results for electrodes with  $N = 24$  atoms, whereas in 6(c) we show results for wider electrodes with  $N = 48$ . The two curves in Fig. 6(a) permit to compare the transmission for two structures with the same aspect ratio  $N_c/N = 12/24$  but different nanoconstriction length  $L$ .



Analogously, Fig. 6(b) shows two  $T(E)$  curves with the same aspect ratio  $N_c/N = 8/24$  and different  $L$ . In Fig. 6(c) we show two  $T(E)$  curves for a wider electrode, keeping the length of the constriction fixed to  $L = 3a$  and changing the aspect ratio. The transmission corresponding to the lowest subband  $|E| < \Delta_1$ , is significantly reduced with respect to the ideal ribbon  $T = 1$ , but remains finite ( $T(0) \simeq 0.18$ ) even for the narrowest and longest constriction.

In order to highlight the peculiar properties of graphene, we give two arguments, which turn out to be inapplicable, to expect a vanishing transmission at zero energy. First, since low energy transmission is associated to edge states and given that the edges of the electrode and the constriction are not connected, the transmission would vanish as  $N_c$  becomes much smaller than  $N$ . This argument fails because the current density of edge states has a sizable contribution in the center of the ribbon, which is smoothly connected to the constrictions considered in Fig. (6). The second argument is based on the behavior of a square constriction with parabolic-band electrons. In that case, the different width of the semi-infinite ribbon  $W_r$  and the constriction  $W_c$  yields different band minima so that an energy gap is created in the narrow region. This can be modeled with square-shaped barrier of height  $V_0 = \frac{\hbar^2}{2m^*} \left( \frac{1}{W_c^2} - \frac{1}{W_r^2} \right)$  and length  $L$ ,  $m^*$  being the effective mass of the electron. The zero energy transmission of a square barrier is always exponentially vanishing with the length, in contrast to our results. This second argument to expect a vanishing transmission at zero energy also fails because the situation for graphene ribbons is very different: Both wide and narrow sectors of the system have zero energy edge states. In other words, it is not possible to create a gap in the low energy region by changing the width of the system so that it is not possible to create a barrier for the carriers in the lowest energy sub-band by geometrical means. Interestingly, the transmission through a square potential has been calculated, in the case of infinitely wide ribbon, and the transmission does not vanish for electrons incident perpendicular to the barrier<sup>27</sup>.

The results in Fig. 6(a) and (b) suggest that the low energy transmission is an increasing function of the constriction width  $N_c$  and and fairly insensitive to constriction length  $L$ . In Fig. 6(d) we plot the transmission at a fixed energy  $E = 0.05t$  as a function of  $N_c/N$  for three families of constrictions. Square symbols correspond to a wide ribbon with  $N = 48$ , and  $L = 3a$ , whereas solid (open) circle symbols correspond to a narrow ribbon with  $N = 24$  and  $L = a$  ( $L = 3a$ ). It is apparent that as the aspect ratio increases, the transmission increases in average, with super-imposed oscillations. This behavior is different from the analogous curve for transmission as a function of the barrier height  $T(E, V_0)$  for parabolic-band electrons in the tunneling regime ( $E < V_0$ ), where the curve does not present oscillations. In the  $E > V_0$  regime the  $T(E, V_0)$  curve can present oscillations<sup>24</sup>. Therefore, the  $T(N_c/N)$  curve looks closer to the latter case, even

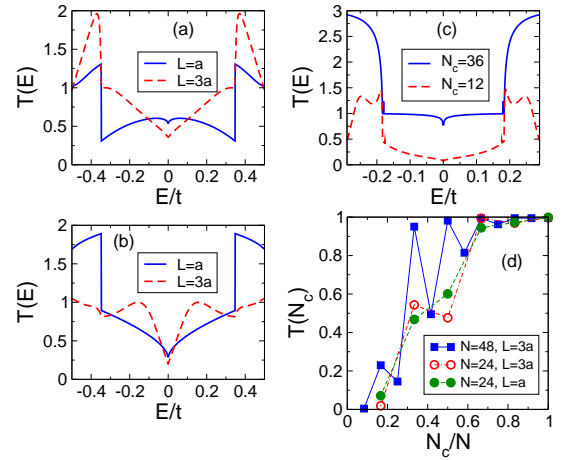


FIG. 6: (Color On-line) Square constrictions. (a)  $T(E)$  curves for the  $N = 24$ ,  $N_c = 12$  and two values of  $L$ . (b)  $T(E)$  curves for the  $N = 24$ ,  $N_c = 8$  and two values of  $L$ . (c)  $T(E)$  curves for  $N = 48$ ,  $L = 3a$  for two constrictions with different  $N_c$ . (d)  $T(E = 0.05t)$  as a function of the aspect ratio of the constriction  $N_c/N$  for 3 families of constrictions.

for very small energy. This is related to the lack of a gap in the density of states. It is also interesting that for both wide and narrow electrodes the transmission saturates to 1 for the same value of  $N_c/N \simeq 0.7$ . As a final remark, only in the case of atomically narrow constrictions the transmission becomes almost zero. In summary, square constrictions are not very efficient in blocking electronic transport in zig-zag graphene ribbons.

## V. WEDGE-SHAPED CONSTRICTIONS

We now turn our attention to a wedge-shaped constriction, shown in Fig. 7. As opposed to the square constrictions considered above, wedge-shaped constrictions are always delimited by zig-zag edges. It can also be expected that wedge-shaped constrictions are more stable than square constrictions, although further work should clarify this point. The structures considered have a top-bottom symmetry, in contrast to the asymmetric structures considered in earlier work<sup>21,22</sup>. Naively, the wedge-shaped constriction would allow for adiabatic transport since the zig-zag edge gets never interrupted. In contrast, we see that for ribbons with  $N = 48$  atoms the constrictions shown in Fig. 7 yield a vanishing transmission in the whole low energy sector  $|E| < \Delta_1$ . We have verified that these results are robust against the removal of a single atom from one of the edges. Surprisingly, these smooth nano-constrictions seem to be more disruptive for low energy transmission than the abrupt nano-constrictions considered in the previous section.

Interestingly, the vanishing transmission is *not* associated to a vanishing density of states in the device region, as shown in Figs. 8(c) and (d). The peaks in the DOS in the energy region with zero transmission is associated

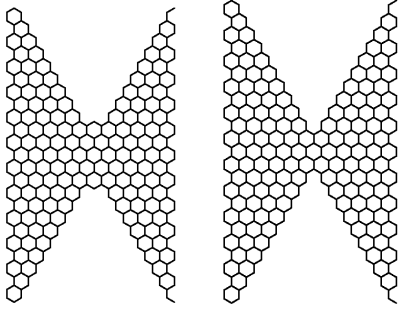


FIG. 7: Schematic atomic structure of wedge-shaped constrictions

with low energy states very weakly coupled, if at all, to the electrodes. The width of the peaks in the DOS is limited by the numerical broadening used in the calculation. In Fig. 9 we show a contour map of the DOS at  $E = 0$  and  $E = 0.04t$ , the energy at which the first peak of the device DOS is located for the structure shown on the right in Fig. 7. The maps reveal localization on the four edges of the constrictions, reflecting the fourfold symmetry of the device. Notice that the LDOS vanishes at the boundary with the electrodes, which explains the vanishing transmission. This LDOS could be observed in STM experiments<sup>19,20</sup>.

Whereas the probability density across one of the four edges has a bell shape for  $E = 0$ , it has a node for the finite energy case. The properties of these low energy non-conducting states in this wedge-shaped structures are very similar to those of zero-dimensional confined states. Confinement in semiconductor heterostructures is associated with the existence of an energy gap. The absence of such a gap in graphene makes it necessary to look for different strategies to confine electrons<sup>27,28,29</sup>. In this regard, nano-constrictions like the ones studied in this section can behave like quantum dots and might permit the study of Coulomb Blockade and Kondo physics in graphene structures. The physical origin of these bound symmetric wedge states (SWS) might be related to the formation of Kekulé vortex structures discussed in the case of asymmetric wedge states<sup>21,22</sup>. In the asymmetric case, the suppression of the transmission occurs for very narrow energy windows, since one of the edges is not perturbed. It would be desirable to study whether the vanishing transmission that we have found is related to the vanishing transmission obtained analytically<sup>27</sup> for the square barrier potential, in infinitely wide ribbons, for incidence angles different from zero. In summary, symmetric wedge constrictions result in a gap in the transmission curve for  $|E| < \Delta_1$ , yet with a finite density of states in that interval, featuring very narrow peaks that mimic a discrete spectrum of confined states.

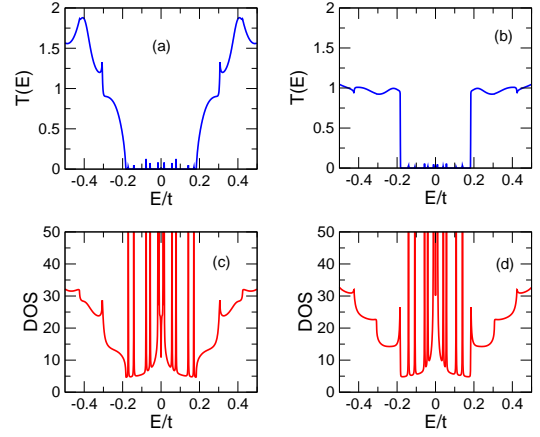


FIG. 8: (Color On-line). (a) and (b)  $T(E)$  for the structures shown in Fig. 7 (blue). (c) and (d) Corresponding density of states projected on the whole constriction region (red).

## VI. DISCUSSION AND CONCLUSIONS

Here we discuss the validity of the approximations assumed for our calculations. Real samples could present several features absent in the idealized ribbon considered here. On one side, the presence of chemical impurities, like hydrogen both in the edge and in bulk, water molecules, oxygen, etc., will affect the electronic structure and transport properties of the system. In a sufficiently clean and ultra-high vacuum environment the effect of chemical impurities could be negligible. In experiments, the graphene ribbon is deposited on an insulating substrate, which has not been included in our calculation. First-principles calculations indicate that the effect of the substrate is weak<sup>30</sup>.

The use of a single-particle model certainly fails, in a trivial sense, if there are deviations from charge neutrality which would make it necessary to perform a self-consistent calculation including, at least, the Hartree contribution. This is certainly achieved by density functional calculations. We have verified that, for the structures considered here, the electronic density does not deviate significantly from charge neutrality. The single par-

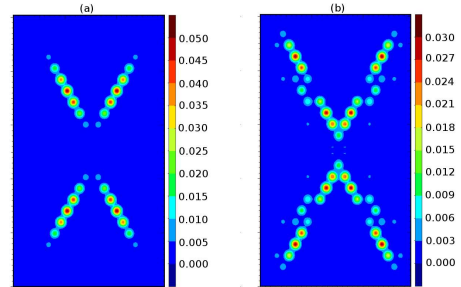


FIG. 9: Local density of states for the right wedge structure shown in Fig. 7 at energies  $E = 0$  (a) and  $E = 0.04t$  (b).

ticle approach also fails if the electron liquid happens to be different from a Fermi liquid, in which the low energy quasiparticles have the same quantum numbers than the free electrons. Such a scenario has been considered for two dimensional graphene<sup>31</sup>. A priori, this is a serious issue in a one dimensional system, where the Fermi liquid state is not stable with respect to electron-electron interaction and a Luttinger liquid is expected. The same statement applies for nanotubes. However, the single-particle Fermi liquid picture describes most of the experimental results in nanotubes and the same can be expected for graphene ribbons.

We have used the same on-site energy (0) and hopping  $t$  for the edge and the inner atoms. This is an approximation, but the results do not change significantly in the case of ideal ribbons<sup>11</sup>. Another limitation of our model is the one orbital approximation. Ab-initio calculations, including all the atomic orbitals, show that the dangling bonds present on the edge atoms form a flat band close to the Fermi energy<sup>23</sup>. We have also ignored the spin degree of freedom. The flat band at zero energy is expected to spin split due to spontaneous magnetization induced by the Coulomb repulsion<sup>23,32</sup>. This interesting issue deserves more theoretical and experimental work. We have also ignored spin-orbit interaction, which is very small in carbon, although it has attracted some interest<sup>33,34</sup>, in part due to the Spin Hall effect<sup>35</sup>.

In summary, we have studied coherent transport in graphene nano-ribbons with zig-zag edges. The electronic structure of the ribbons is described with a simple one orbital tight-binding approximation. We have focused on narrow ribbons ( $W < 5nm$ ) for which only the lowest energy sub-band is expected to be experimentally

relevant. Our results could be summarized as follows: *i)* The low-energy transport properties are robust with respect to isolated vacancies on the edges. *ii)* These are also robust with respect to square-shaped nano-constrictions. Linear conductance survives in most cases except for very narrow constrictions. This is at odds with the behavior of parabolic-band electrons in similar constrictions and reflects two non-trivial features of edge states: Their minimum energy is independent of the ribbon width and their current density profile spreads beyond the edges of the ribbon, in contrast with their density profile. *iii)* In contrast to square constrictions, wedge-shaped nano-constrictions result in a gap in the transmission and result in a zero linear conductance which is related to the appearance of localized low energy edge states. These edge states have properties similar to those of confined states in zero dimensions. Therefore, graphene wedge shape constrictions might have properties analogous to those of semiconductor quantum dots. Extensions of this work will address the spin degree of freedom, topological defects<sup>36</sup> and armchair edges.

We acknowledge useful discussions with M. Vozmediano, A. Cortijo and B. Valenzuela. This work has been financially supported by MEC-Spain (Grants FIS200402356, MAT2005-07369-C03-01 and the Ramon y Cajal Program) and by Generalitat Valenciana (GV05-152). This work has been partly funded by FEDER funds.

*Note added:* After the completion of this work we have been aware of a related theory paper<sup>37</sup> with transport calculations in wedge-shape nano-constrictions similar to that of figure (7).

- 
- <sup>1</sup> J. Scott-Bunch *et al.*, Nanoletters **5** 287 (2005)
  - <sup>2</sup> K. S. Novoselov *et al.*, Nature **438**, 197 (2005).
  - <sup>3</sup> Y. Zhang *et al.*, Nature **438**, 201 (2005).
  - <sup>4</sup> C. Berger *et al.*, Science **312**, 1191 (2006)
  - <sup>5</sup> M. I. Katsnelson, Eur. Phys. J. **51**, 157 (2006)
  - <sup>6</sup> J. Tworzydło, B. Trauzettel, M. Titov, A. Rycerz, C.W.J. Beenakker Phys. Rev. Lett. **96** 246802 (2006)
  - <sup>7</sup> Kentaro Nomura, A.H. MacDonald, cond-mat/0606589
  - <sup>8</sup> G. W. Semenoff, Phys. Rev. Lett **54**, 2449 (1984)
  - <sup>9</sup> K. Nakada, M. Fujita, G. Dresselhaus and M. S. Dresselhaus, Phys. Rev. B **54**, 17954 (1996)
  - <sup>10</sup> K. Wakabayashi, M. Fujita, H. Ajiki, M. Sigrist, Phys. Rev. B **59**, 8271 (1999)
  - <sup>11</sup> M. Ezawa, Phys. Rev. B **73**, 045432 (2006).
  - <sup>12</sup> L. Brey and H. Fertig, Phys. Rev. B **73**, 235411(2006)
  - <sup>13</sup> N. M. R. Peres, A. H. Castro Neto, and F. Guinea Phys. Rev. B **73**, 195411 (2006) N. M. R. Peres, A. H. Castro Neto, and F. Guinea Phys. Rev. B **73**, 239902 (2006)
  - <sup>14</sup> *Physical Properties of Carbon Nanotubes*, R Saito, M S Dresselhaus, G Dresselhaus, World Scientific, Singapore (1998)
  - <sup>15</sup> A. Javey, J. Guo, Q. Wang, M. Lundstrom and H. Dai Nature **424**, 654 (2003)
  - <sup>16</sup> P. Jarillo-Herrero, S. Sapmaz, C. Dekker, L.P. Kouwenhoven LP, van der Zant H. Nature **429** 389 (2004)
  - <sup>17</sup> J. Nygard, D. H. Cobden, P. E. Lindelof Nature **408**, 342 (2000)
  - <sup>18</sup> P. Jarillo-Herrero, J. Kong, H. van der Zant, C. Dekker, L.P. Kouwenhoven, S. De Franceschi Nature, **434**, 484 (2005)
  - <sup>19</sup> Y. Niimi, T. Matsui, H. Kambara, K. Tagami, M. Tsukada, and H. Fukuyama, Appl. Surf. Sci. **241**, 43 (2005).
  - <sup>20</sup> Y. Kobayashi, K. I. Fukui, T. Enoki, K. Kusakabe, and Y. Kaburagi, Phys. Rev. B **71**, 193406 (2005).
  - <sup>21</sup> K. Wakabayashi and M. Sigrist, Phys. Rev. Lett. **84**, 3390 (2000)
  - <sup>22</sup> K. Wakabayashi, Phys. Rev. B **64** 125428 (2001)
  - <sup>23</sup> Y. Miyamoto, K. Nakada, and M. Fujita, Phys. Rev. B **59**, 9858 (1999);  
H. Lee *et al.*, Chem. Phys. Lett. **398**, 207 (2004)  
Takazumi Kawai, Yoshiyuki Miyamoto, Osamu Sugino, and Yoshinori Koga Physical Review B **62**, R16349 (2000)
  - <sup>24</sup> S. Datta, *Mesoscopic Transport*.
  - <sup>25</sup> D. Gunlycke, H. M. Lawler, C. T. White, cond-mat/0606693
  - <sup>26</sup> V. V. Cheianov, V. Falko, cond-mat/0603624



- <sup>27</sup> M. I. Katsnelson, K. S. Novoselov, A. K. Geim, cond-mat/0604323
  - <sup>28</sup> P.G.Silvestrov, K.B.Efetov, cond-mat/0606620
  - <sup>29</sup> J. Milton Pereira Jr., V. Mlinar, F. M. Peeters, P. Vasilopoulos, Phys. Rev. B **74**, 045424 (2006)
  - <sup>30</sup> B. Obradovic, R. Kotlyar, F. Heinz, P. Matagne, T. Rakshit, M. D. Giles, M. A. Stettler, and D. E. Nikonov Appl. Phys. Lett. **88**, 142102 (2006)
  - <sup>31</sup> J. González, F. Guinea, and M. A. H. Vozmediano Phys. Rev. Lett. **77**, 3589-3592 (1996)
  - <sup>32</sup> M. A. H. Vozmediano, M. P. Lopez-Sancho, T. Stauber, F. Guinea Phys. Rev. B **72**, 155121 (2005) N. M. R. Peres, F. Guinea, A. H. Castro Neto Phys. Rev. B **72**, 174406 (2005)
  - <sup>33</sup> L. Chico, M. P. López-Sancho, and M. C. Muñoz Phys. Rev. Lett. **93**, 176402 (2004)
  - <sup>34</sup> D. Huertas-Hernando, F. Guinea, A. Brataas, cond-mat/0606580
  - <sup>35</sup> C.L. Kane, E.J. Mele, Phys. Rev. Lett. **95**, 226801 (2005),
  - <sup>36</sup> Alberto Cortijo, M. A. H. Vozmediano, cond-mat/0603717
  - <sup>37</sup> A. Rycerz, J. Tworzydło, C. W. J. Beenakker, cond-mat/0608533
-